Chapter 11
Computer Programs and Application Data

This chapter presents an overview of the computer programs *Thermal* and *Reflective*. Both programs have help files that describe individual inputs. This chapter does the following:

1. describes the physical models and assumptions implemented in the programs,
2. provides suggestions for modeling the MTF of objective lenses,
3. explains the interface to the detector data described in Chapter 12, and
4. suggests ways to use the programs to evaluate imager performance.

The programs are included for two reasons. First, the programs help the design engineer or systems analyst make imager design trades. The book provides suggestions for modeling optics and displays. The characteristics of available thermal FPAs are directly coupled to the *Thermal* computer program speed performance analysis. The computer programs are designed to provide quick but physically reasonable performance estimates.

The second reason for including the programs is to let the reader experiment with the theory. Blur, noise, and aliasing interact with target size and contrast to establish performance. For a given imager design, the relative importance of each factor is probably not obvious. For example, the dependency of aliasing on blur is clear from the theory. But the impact or importance of aliasing is not clear until the reader runs specific examples. The programs allow the user to vary imager and target characteristics while observing the effect on imager resolution.

Section 11.1 provides suggestions for estimating optical MTF. Section 11.2 provides estimates for the blur associated with the most common display technologies. Section 11.3 discusses the effect of atmosphere on performance and describes modeling assumptions. *Thermal* recalculates detectivity for each background temperature input by the user. The detectivity algorithms used in the program are summarized in Section 11.4. Both *Thermal* and *Reflective* models calculate diffusion MTF as well as spatial MTF for detectors. Detector MTF calculations are also described in Section 11.4. Section 11.5 explains computer program inputs and outputs. Section 11.6 offers suggestions for using the programs to analyze imager performance.

11.1 Optics Modulation Transfer Function

This section provides suggestions for modeling objective lens MTF. Many optics design programs such as CODE V, ZEMAX, and OLSO are available. Some of the numerous books covering optical design are listed in the bibliography. By far, the best procedure for modeling optical MTF is to use these programs in the manner explained in the literature.

In the early stages of system design, however, the output from optical design programs is not available. In the absence of better information, diffraction-limited performance is often assumed. In the MWIR and LWIR, assuming ideal MTF is reasonable for many lenses. The discussion in Section 11.1.1 describes when the ideal can be assumed and what to use for MTF in other cases. Broadband imagers operating in the visible, NIR, and SWIR do not achieve diffraction-limited performance. Section 11.1.2 provides MTF estimates for objective lenses operating in the NIR and SWIR spectral bands.

11.1.1 Thermal imagers

This section provides suggestions for modeling a thermal objective lens. Diffraction-limited performance is sometimes a realistic assumption. The computer model allows the user to easily select other options. This section describes those options and their applicability.

When designing thermal objectives, a number of factors must be considered. Producibility, weight, and volume are all important factors. Athermalization and performance over temperature extremes must be considered. Narcissus limits design options. Due to the high cost of infrared materials and their relatively poor transmission, lens thickness should be minimized. For cryogenic detectors, effective cold shielding is important for reducing detector noise. Most often, the system has multiple fields of view. These design considerations are all important and often require either compromising MTF or increasing the complexity and expense of the optical design.

Figure 11.1 shows MTFs for several production systems versus their diffraction limit. All of these systems except one operate in the MWIR. The abscissa is spatial frequency normalized to the diffraction limit for each optical system. The ordinate is MTF. The labels represent *f*/#, field of view, and whether the MTF is for on-axis (on) or off-axis (off). For example, "*f*/6, 1.5, off" represents an optical system with a 1.5-deg field of view using *f*/6 optics. Field of view is full angle. The "off" means the MTF is for an off-axis field angle of 0.7 of full field. For this example, the field angle is 0.525 deg. The notation "Tmp" means temperature. These MTFs are for a field angle equal to 0.7 of full field and at a temperature extreme of 70 °C.

All of the MWIR data in Figure 11.1 are predicted by optics design programs. The *f*/1.1 LWIR lens MTF is a Gaussian fit to measured data. Degradation due to nonideal spacing or alignment is not included in the MWIR estimates. However, measured data are available at lower spatial frequencies for

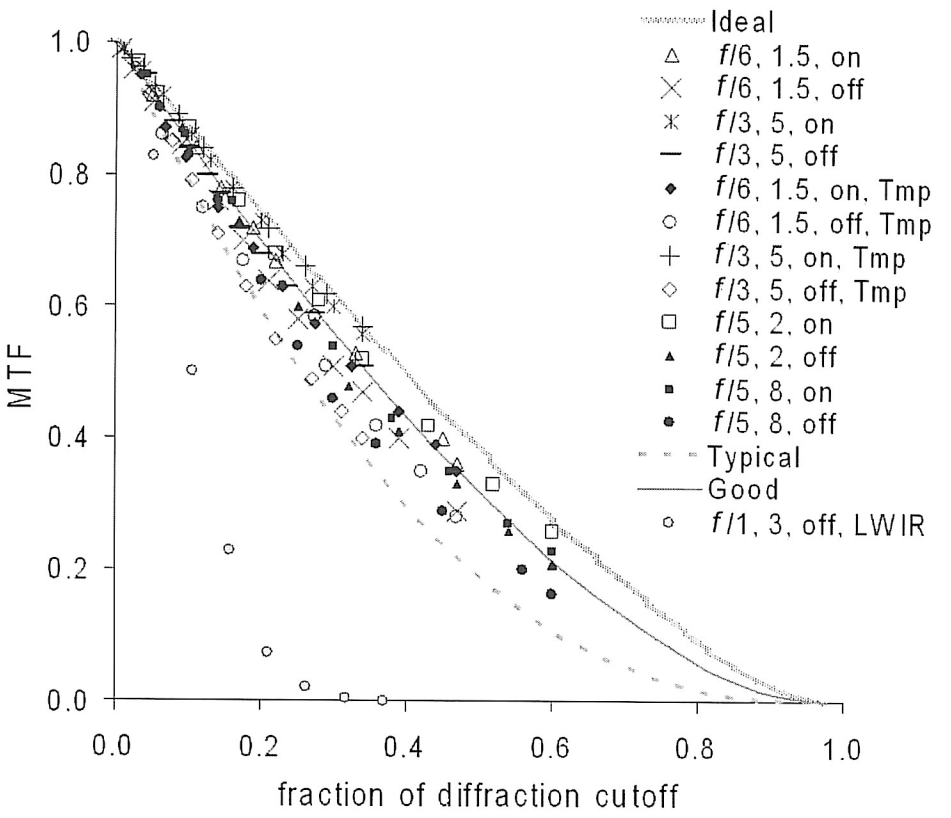

Figure 11.1 MTF for several MWIR objective lenses and one LWIR objective lens. The abscissa is spatial frequency normalized to diffraction cutoff for each lens. The LWIR MTF is a Gaussian fit to measured data. All of the other MTFs are predicted by optics design programs. The labels refer to *f*/#, full field of view in degrees, and on- or off-axis. "Tmp" means that MTFs are for off-axis and at a temperature of 70 °C.

the *f*/6 and *f*/3 lenses, and that measured data supports the MTF predictions. Available data are sparse at higher spatial frequencies due to the habit of not presenting MTF values beyond the half-sample frequency. The half-sample frequency depends on the detector array used. Signal at frequencies beyond "Nyquist" creates aliasing, and these MTF values are important in analyzing system performance. Nonetheless, published data tends to omit this information.

The ideal and good curves in Figure 11.1 bracket on-axis MTF for *f*/3 or higher optics. Off-axis performance and especially degradation due to temperature are bracketed by the good and typical curves. The name typical derives from the idea that off-axis and non-room-temperature environments represent the typical operational usage. For systems with fields of view larger than perhaps 15 deg, the typical MTF curve is probably optimistic.

Figure 11.2 compares the model ideal, good, and typical curves to design examples suggested by Fischer and Tadic-Galeb[1] and by Smith.[2] Design details for the examples are given in Table 11.1. Except for the *f*/0.75 lens, all of these

examples use achromatic doublets with a field-flattening lens. Only Optic 6 provides 100% cold shielding of the detector. All designs are for a wide spectral band except for Optic 6; that lens provides poor MTF for the wide 3–5-μm spectral band. These objectives are simpler than designs found in real systems. Production systems provide 100% cold shielding and multiple fields of view by using more lens elements to achieve equivalent performance.

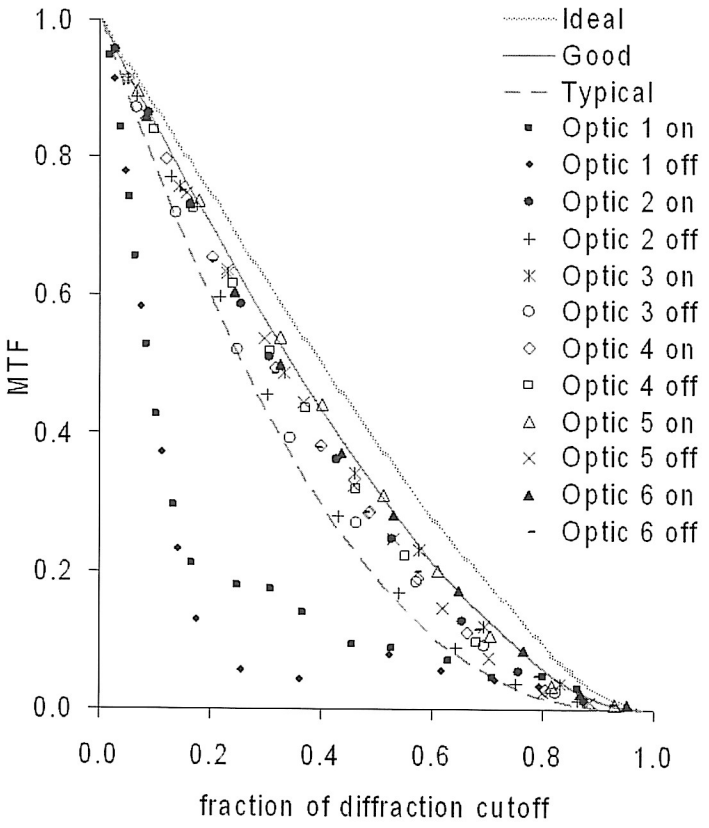

Figure 11.2 Lens design examples compared to model fits. The abscissa is spatial frequency as a fraction of diffraction cutoff for each lens. Ordinate is MTF.

Table 11.1 Design details for objective lenses. MTF for these lenses is shown in Fig. 11.2.

Optic	*f*/#	FOV (degrees)	focal length (cm)	spectral band (μm)	cold shield
1	0.75	6	10	8–12	no
2	1.5	3	16.5	8–12	no
3	1.5	12	10	3–5	no
4	3	2	10	8–12	no
5	3	12	10	3–5	no
6	3	3	10	3.6–4.2	yes

In Figure 11.2, the good and typical model curves bracket all of the MTFs except for the very fast (*f*/0.75) MWIR lens. MTF for high *f*/# and on-axis tends toward the good model. Low *f*/# and off-axis MTF is represented by the typical model curve.

In general, the ideal is easier to achieve in the LWIR than in the MWIR because surface errors are a smaller fraction of wavelength. For most optical designs, the ideal is easier to achieve on axis than off axis. Approaching the ideal is easier for large *f*/#s and smaller fields of view.

The thermal program allows the user to input optics MTF if it is available. Also, the user can select ideal, good, or typical. The MTF used by the program in each case is shown in Figs. 11.1 and 11.2 and given by Eqs. (11.1) through (11.3). Perhaps the best use of the typical, good, and ideal inputs is to run the program once using each option in order to understand the importance of the optical MTF in establishing overall imager resolution.

Ideal MTF is given by Eq. (11.1). The good and typical MTF curves are obtained by raising the diffraction MTF to the 1.2 power and 1.75 power, respectively. This is shown in Eqs. (11.2) and (11.3). Only horizontal MTF is shown; similar formulas are used for vertical MTF.

$$H_{x-diff}(\xi) = \frac{2}{\pi}\left[\cos^{-1}\left(\frac{1000\xi\lambda}{D}\right) - \frac{1000\xi\lambda}{D}\sqrt{1-\left(\frac{1000\xi\lambda}{D}\right)^2}\right]$$
$$\text{for } \frac{1000\xi\lambda}{D} < 1, \; H_{x-diff}(\xi) = 0 \quad \text{for } \frac{1000\xi\lambda}{D} \geq 1, \tag{11.1}$$

where

ξ is horizontal spatial frequency in $(\text{mrad})^{-1}$,
D is aperture diameter in meters,
λ is wavelength in meters, and
$H_{x\text{-}diff}$ is the horizontal diffraction MTF.

$$H_{x-good}(\xi) = \left[H_{x-diff}(\xi)\right]^{1.2}. \tag{11.2}$$

$$H_{x-typical}(\xi) = \left[H_{x-diff}(\xi)\right]^{1.75}. \tag{11.3}$$

11.1.2 Imagers of reflected light

This section provides suggestions for modeling objective lens MTF for reflected-light imagers. The emphasis here and in the reflected-light computer program is on broadband passive imagers operating in the NIR and SWIR that use monochrome displays. The orientation is on long-range target acquisition, security, and mobility imagers.

Optics for passive imagers operating in the visible, NIR, and SWIR do not achieve diffraction-limited performance. Figure 11.3 shows MTF for several production lenses versus diffraction limit. The *f*/1.2 wide field-of-view (WFOV) imager has a 40-deg field of view. The spectral band is 0.6 to 0.9 μm. The *f*/2 SWIR optic has a 9-deg field of view and operates from 0.9 to 1.7 μm. The *f*/5 SWIR is the only reflective optic in this set and has a 2-deg field of view. The *f*/4 SWIR has a 10-deg field of view with a spectral band from 0.9 to 2 μm. As with the thermal examples, data are sparse at higher spatial frequencies due to the habit of not reporting MTF beyond the half-sample frequency.

Figure 11.3 shows the three model inputs available in the computer program: good, typical, and WFOV. The "book typical" curve shown in Fig. 11.3 is taken from Fig. 10.10 of Ref. 1. Only the reflective *f*/5 SWIR optic comes close to the good model and then only on the optical axis and at a fraction of the diffraction cutoff frequency. Off-axis performance for reflective and all of the narrow field-of-view refractive optics is represented by the typical model. For fields of view greater than about 10 deg, the WFOV model is used. These MTF curves are intended to be physically reasonable.

As with the thermal model, optics MTFs can be input by the model user. This is the best approach if the information is available.

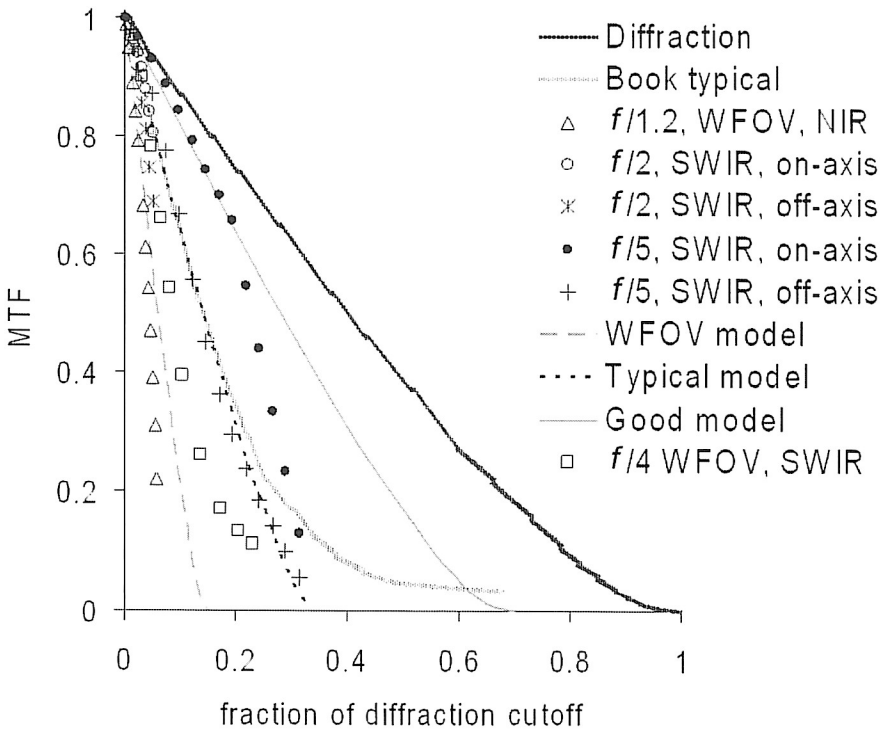

Figure 11.3 MTF of several NIR and SWIR objectives compared to model approximations. The abscissa is spatial frequency normalized to diffraction cutoff for each lens. Ordinate is MTF.

The good, typical, and WFOV model curves are based on diffraction MTF. Equation 11.4 gives the model MTF. The values of Ω are 0.7, 0.35, and 0.15 for good, typical, and WFOV, respectively.

$$H_{x-optic}(\xi,\Omega)=\frac{2}{\pi}\left[\cos^{-1}\left(\frac{1000\xi\lambda}{\Omega D}\right)-\frac{1000\xi\lambda}{\Omega D}\sqrt{1-\left(\frac{1000\xi\lambda}{\Omega D}\right)^2}\right]$$
$$\text{for } \frac{1000\xi\lambda}{\Omega D}<1,\ H_{x-optic}(\xi,\Omega)=0 \text{ for } \frac{1000\xi\lambda}{\Omega D}\geq 1. \tag{11.4}$$

11.2 Display Modulation Transfer Function

This section describes how display MTF is calculated in the computer programs. Four display options are provided. These include high-resolution monochrome cathode ray tube (CRT), color CRT, color liquid crystal display (LCD), and high-resolution monochrome LCD. The color CRT also represents a low-resolution monochrome display. The primary market for the monochrome LCD displays is medical, so these are referred to as medical displays.

11.2.1 Cathode ray tubes

CRT technology is highly developed. Blur size is proportional to display size for diagonal dimensions from 1 to 30 in or more. Modern CRTs present a flat field that is free of line raster and other artifacts.

CRT blur is modeled as Gaussian.[3] Blur size is obtained using the shrinking raster dimension.[4] That is, the lines are spaced just close enough that raster disappears. This assumption provides two performance advantages. First, it maximizes appearance even when the observer is close to the display. Second, it provides the minimum blur size compatible with the flat-field assumption.

For a line pitch s millimeters (mm), spot blur MTF H_{spot} is given by Eq. (11.5). Spatial frequency ξ_{mm} is in cycles per millimeters on the display. Line spacing s is based on display height in millimeters divided by 525 lines for a low-resolution CRT and 960 lines for a high-resolution CRT.

$$H_{spot}(\xi_{mm})=\exp(-5.8s^2\xi_{mm}^2). \tag{11.5}$$

The user provides the diagonal dimension of the display. The program calculates display height based on a height-to-width ratio of three to four for most displays. For the high-definition television (HDTV) format, a nine-to-sixteen ratio is assumed. The dimension s is then obtained by dividing display height by either 525 or 960, depending on display resolution.

The shrinking-raster assumption is probably optimistic in most cases. The great variety of available CRT displays makes a definitive statement impossible.

However, Figs. 11.4 through 11.6 compare model results to measurement results from the author's experience.

Figure 11.4 compares the shrinking-raster assumption to measurements of a head-up display (HUD) CRT. The HUD uses a 1-in display viewed through a glass combiner and eyepiece. The video format is high resolution at 875 lines. The measurement data are taken through the combiner; this might explain the poor MTF at low spatial frequencies. The sharp drop near zero frequency is likely due to halation. The model line provides a somewhat optimistic but reasonable estimate of the Gaussian blur spot MTF. If the user is aware of additional MTF losses due to halation or contrast loss in the combiner, these can be included as additional post-MTFs.

Figure 11.5 compares model MTF to measurements of a color CRT display. Pixel pitch is 0.38 mm (67 lines per in). The data are represented by Gaussian curve fits. Unfortunately, the original data points are not available. Again, the model is reasonable although somewhat optimistic.

Figure 11.6 compares model to measurements on a high-resolution monochrome medical display. The line pitch in this case is 0.14 mm (180 lines per in). Again, the data are represented by a Gaussian fit. The model is quite optimistic in this case. Apparently, the video lines are closer together than in the shrinking-raster assumption.

The shrinking-raster assumption is optimum in the sense that blur spot size is minimized while maintaining a flat field. The flat field avoids aliasing generated at the display. The user has the option to add post-MTF and compensate for the optimistic display. However, good information on display MTF is generally not publicly available. The model provides a default Gaussian spot that optimizes the display but is physically reasonable.

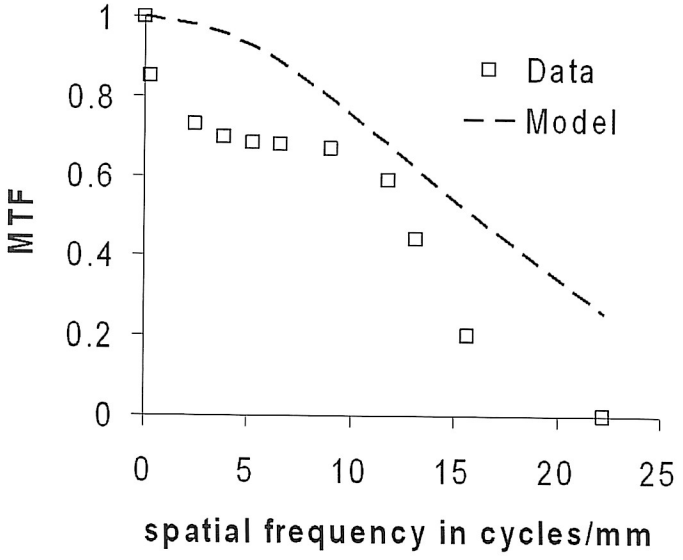

Figure 11.4 Model versus MTF data for a high-resolution HUD display.

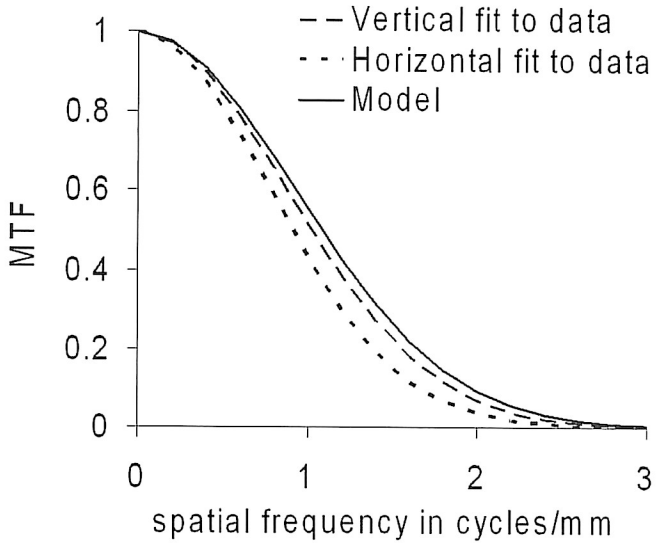

Figure 11.5 Measured MTF of color display compared to model prediction. The measured data are represented by Gaussian curve fits. The model prediction is reasonably close.

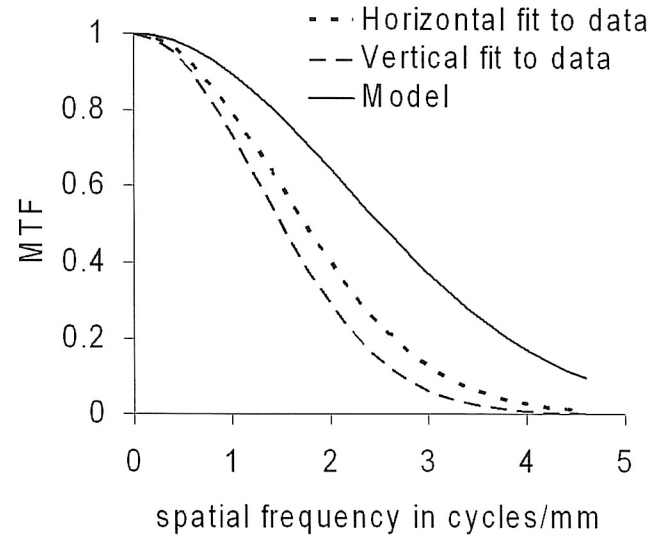

Figure 11.6 Comparison of model MTF to data for a monochrome medical display. The data are represented by Gaussian fits. The model is optimistic.

CRT MTF is also degraded by a horizontal sample and hold circuit. Using H_{pit} for horizontal pitch in mm, sample and hold MTF H_{SH} is given by Eq. (11.6):

$$H_{SH}(\xi_{mm}) = \frac{\sin(\pi \xi_{mm} H_{pit})}{\pi \xi_{mm} H_{pit}}. \tag{11.6}$$

11.2.2 Liquid crystal displays

Figure 11.7 shows a schematic of a color LCD unit cell.[6] This unit cell represents a high-aperture-ratio design. The active areas have a larger fill factor than most LCD displays sold today. The unit cell is small. The blue-, green-, and red-emitting areas are in close proximity. The eye cannot resolve the individual colored areas. Therefore, the cell produces one color, and that color depends on the relative amount of red, green, and blue light. White is produced by the relative intensities shown by the dashed lines in Fig. 11.8. Since the display is used to present a monochrome image, cells produce only white light in the model.

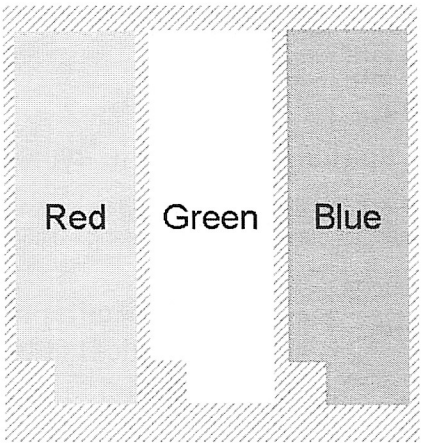

Figure 11.7 Illustration of an LCD unit cell. A high-aperture-ratio cell is shown.

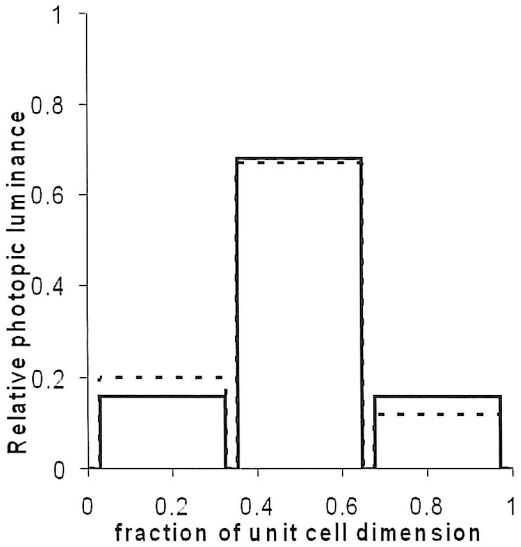

Figure 11.8 The dashed line shows relative luminance for each color cell to produce white light. The solid line shows the intensity profile used in the model.

The model permits only real MTFs. The dashed-line intensity pattern in Fig. 11.8 is not symmetrical; therefore, the MTFs are complex. The relative intensities shown by the solid line are used to model color LCD MTFs. Color LCD MTFs are shown in Fig. 11.9. These MTFs are for a unit cell dimension of 1 mm. The formulas for horizontal MTF H_{LCD} and vertical MTF V_{LCD} for a color LCD are given by Eqs. (11.7) and (11.8). H_{pit} is cell size in millimeters. The width of a color cell is 0.29 H_{pit}. The offset of the blue and red cells from the center is 0.32 H_{pit}. The vertical dimension of the color cells is 0.85 H_{pit}.

$$H_{LCD}(\xi_{mm}) = \frac{\sin(0.29\pi\xi_{mm}H_{pit})}{0.29\pi\xi_{mm}H_{pit}}[0.68 + 0.32\cos(0.64\pi\xi_{mm}H_{pit})]. \quad (11.7)$$

$$V_{LCD}(\xi_{mm}) = \frac{\sin(0.85\pi\xi_{mm}H_{pit})}{0.85\pi\xi_{mm}H_{pit}}. \quad (11.8)$$

The same cell construction is used for medical LCDs except that the color filters are removed. The three color cells are illuminated independently in order to obtain better amplitude quantization. This means that white-light MTF varies with intensity. For the purposes of the model, the three amplitudes are assumed to be equal. The vertical MTF for the medical LCD is given by Eq. (11.8). The horizontal MTF is given by Eq. (11.9). Medical LCD MTF is also shown in Fig. 11.9.

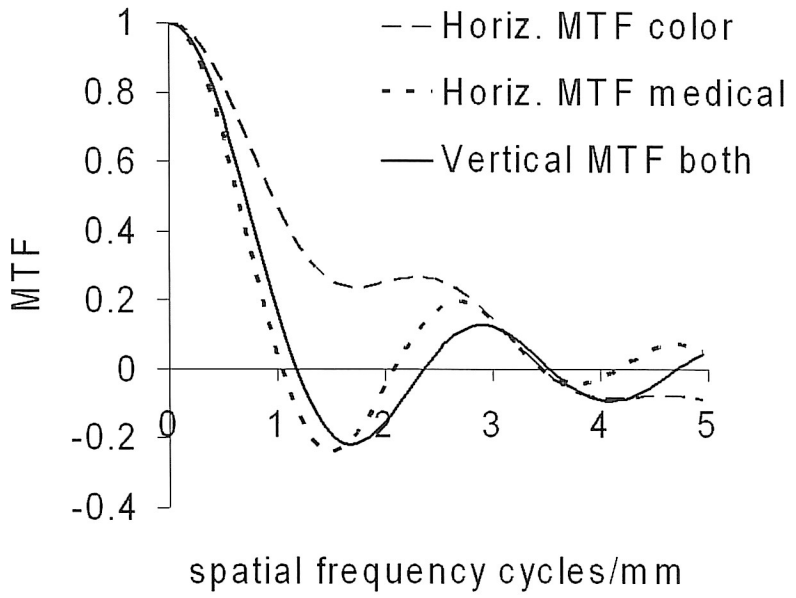

Figure 11.9 MTFs for LCD displays. The MTFs shown are for a unit cell dimension of 1 mm. Horizontal color is the dashed line. Horizontal medical is the dotted line. Vertical MTFs for both types of display are shown by the solid line.

$$H_{LCD}(\xi_{mm}) = \frac{\sin(0.29\pi\xi_{mm}H_{pit})}{0.29\pi\xi_{mm}H_{pit}}[0.33 + 0.67\cos(0.64\pi\xi_{mm}H_{pit})]. \quad (11.9)$$

Willem den Boer provides a clear discussion of available LCD technologies in Ref. 6. He also describes the sources of motion blur and explains how LCD televisions minimize motion blur.

11.2.3 Display interface format

Display interface options are shown in Table 11.2.

Table 11.2 Display interface options.[5]

Description	Standard	Horiz. pixels	Vert. lines	Inter-lace	Frame rate in Hertz
U.S. analog video (RS-170)	NTSC	640	480	Yes	60
High-resolution analog video	RS-343	1280	960	No	50 or 60
HDTV		1280	720	No	60
Computer	VGA series	any	any	No	50 or 60
European analog video	PAL	768	576	Yes	50
European component digital video		720	483	No	50

11.3 Atmospheric Transmission and Turbulence

Expected environment is one important factor in selecting an imager for a task. For example, atmospheric transmission in a high-humidity hot environment is better for MWIR than for LWIR. On the other hand, the longer wavelengths of LWIR improve turbulence MTF. The program provides a selection of atmospheres so that the user can evaluate the impact of atmosphere on imager performance.

The objective of imager analysis is to optimize future performance during a variety of tasks in unknown locations and unpredictable weather. For this reason, the program allows the user to easily change target set characteristics, atmospheres, and backgrounds in order to evaluate the imager under diverse conditions.

Generating a PID-versus-range curve for one atmosphere and for a single target contrast and dimension provides little information about future capability. For example, depending on weather and time of day, the thermal signature for nonexercised targets ranges from 0.1 to more than 10 K. Evaluating imager performance at 1 or 2 K leads to a myopic view of sensor performance.

When predicting contrast transmission, certain assumptions are made consistent with the nature of these models. One assumption is that the target and background are colocated. The target is viewed against local terrain. Distance to the target and to the background are the same. A second assumption is that the average flux seen by the imager does not change with range. User selection of background characteristics establishes background flux.

In reality, path radiance results in range-dependent background flux. This is particularly true in the reflective spectral bands. This means that both imager noise and target contrast are range dependent. Implementing range-dependent flux provides marginally better accuracy in the probability-versus-range curve. Range errors using the constant-flux model are small in the thermal bands. Range errors are largest in the reflective bands and for high sky-to-ground ratios (SGRs).

The objective of these models is to quantify imager resolution. Our view is that implementing the range-dependent model confounds the impact of multiple important factors without significantly improving range prediction accuracy. The simplified model allows the user independent control of both background flux and target signature. The program permits the user to stimulate the imager with a variety of realistic background and target signatures. The exact range at which a target might present the combination of signal and noise is not significant. What is significant is the ability of the imager to manage the diverse situations that will be encountered during years of use. Our goal is to provide the user insight into imager capabilities. The next two sections provide details on implementing the reflective and thermal models.

11.3.1 Atmosphere in the reflective model

Light from the sun, moon, and stars passes through the atmosphere before illuminating the target and background. Absorption bands in the atmosphere act on the light before the light reflects from ground objects. Light absorbed by the atmosphere is not present in the illumination spectra. In the reflective spectral bands, atmospheric absorption has little effect on horizontal path transmission.

Contrast is reduced by aerosol scattering of target signal out of the line of sight. Contrast is also reduced by sunlight, moonlight, or starlight scattered by aerosols into the imager's field of view. See Fig. 11.10 for an illustration. In most scenarios, path radiance resulting from light scattered into the sensor's path is the most serious cause of target-to-background contrast loss.

The atmospheric path can appear brighter at the imager than at the zero-range target and background. This results in substantial loss of contrast. Path radiance is quantified by the SGR. As the atmospheric path lengthens, the path becomes brighter. At some point, the path becomes optically thick. That is, only light from the path is seen, and increasing the path length does not change the path radiance. The SGR is the ratio between the maximum path radiance and the zero-range radiance. SGR does not vary with range because the peak long-range value is used in the ratio. Figure 11.11 shows the effect of SGR on contrast transmission. Table 11.3 gives values of SGR for a variety of terrains and cloud cover.

Equation 11.10 is used to calculate contrast loss for range R_{ng}, Beer's law coefficient β, and target zero-range contrast $C_{tgt\text{-}0}$:

$$C_{TGT} = \frac{C_{TGT-0}}{1 + SGR\left(\beta^{-R_{ng}} - 1\right)}. \tag{11.10}$$

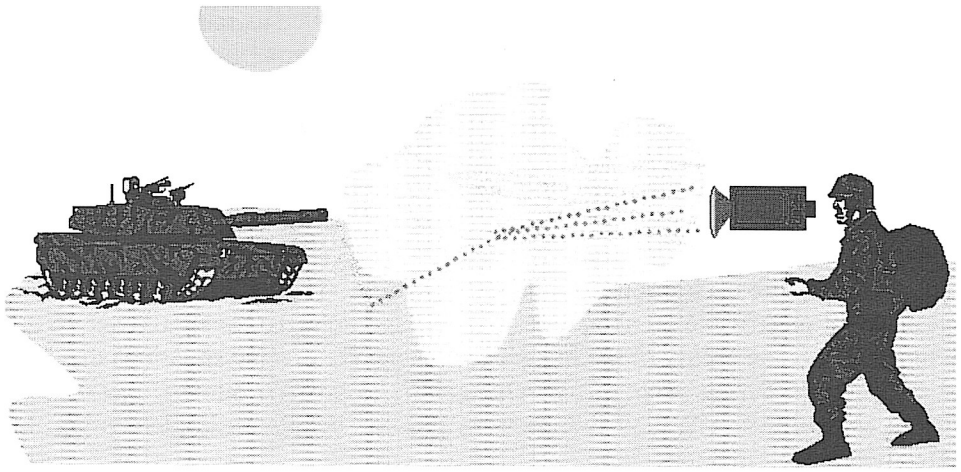

Figure 11.10 Sunlight scattered from atmosphere degrades target-to-background contrast.

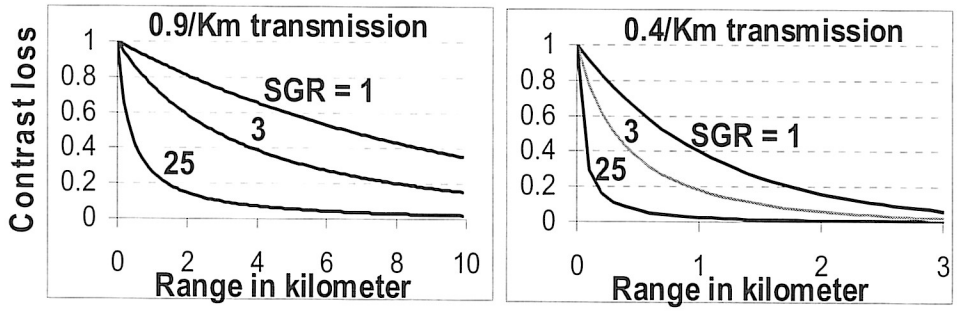

Figure 11.11 Effect of SGR on contrast transmission. The graph on the left shows the effect when the Beer's law transmission is 0.9 per km. The graph on the right shows the effect with 0.4-per-km transmission.

Table 11.3 Typical SGR ratios.

Terrain	Clear	Overcast
Desert	1.4	7
Forest	5	25
Typical	3	

Given knowledge of the path transmission and SGR, Eq. (11.10) is used to obtain target contrast at range. SGR is difficult to estimate, however, and a more empirical approach is used in the computer program.

Visibility is affected by both path transmission and SGR. Visibility is the range at which an observer can just distinguish a high-contrast target. However, visibility range cannot be used directly, because transmission through aerosols improves as wavelength increases. A method is needed to predict the wavelength dependency of contrast loss. The empirical method described by Waldman and Wootton is used in the *Reflective* program.[7] In Eq. (11.11), visibility V and range R_{rg} are both in kilometers. The extinction coefficient is V_{ext}. The center wavelength of the spectral band is λ_{center}.

$$
\begin{aligned}
Q &= 0.585V^{0.3333} \quad \text{for } V \leq 7 \text{ km.} \\
Q &= 0.006583V + 1.07 \quad \text{for } V > 7 \text{ km.} \\
V_{ext} &= \frac{3.91\left(\dfrac{0.55}{\lambda_{center}}\right)^{Q}}{V}. \\
\beta &= \exp(-V_{ext}).
\end{aligned}
\tag{11.11}
$$

The model user inputs visibility (obviously in the visible band!), and the model calculates β for the imager's spectral band.

11.3.2 Atmosphere in the thermal model

MODTRAN 4 is the *de facto* standard for predicting transmission. However, it is not feasible to include MODTRAN in the program distribution. For that reason, five combinations of standard atmospheres and visibilities are included as transmission tables. The transmissions are calculated for horizontal paths only.

Type 1: U.S. Standard 1976 rural with 23-km visibility
Type 2: Tropical (15 N Latitude) Navy maritime aerosol
Type 3: Sub-Arctic winter with no aerosol
Type 4: Midlatitude winter with urban 5-km visibility
Type 5: Midlatitude summer, desert extinction

The one-wavenumber (cm^{-1}) MODTRAN transmissions are filtered with a triangular slit (40 cm^{-1} full-width half-maximum) and then sampled at 20 cm^{-1}. There are 642 values at each range covering the 2.5- to 13.5-μm spectral band. The data are stored for ranges 0.1, 0.3, 0.5, 1, 3, 7, 10, 20, and 50 km. A logarithmic interpolation at each wavenumber is used to obtain transmissions for intermediate ranges. The RMS errors associated with range interpolation are

The detector flux environment is illustrated in Fig. 11.15. In A at the top, the detector is effectively cold shielded. All of the light hitting the detector is from the scene, with the exception of any light radiated from the lens itself. In B at the bottom of the figure, the cold shield allows light radiated from the enclosure to hit the detector. The flux on the detector depends on enclosure temperature as well as on scene temperature. Cold shielding is not effective, and enclosure temperature affects detector noise.

The physical constants used in the equations are discussed in *The Infrared Handbook*[10] and many other books on radiometry and Planck's blackbody equation. The origin of the constants is not described here. The following parameters, constants, and units are used in the equations:

C1 = 37,418 W μm^4 cm^{-2},
C2 = 14,389 μm K,
C3 = 2E–19 J μm,
$q_e = 1.6 \times 10^{-19}$ C (coulomb) (the charge on an electron),
λ = wavelength in microns,
λ_0 = start wavelength of spectral band,
λ_1 = stop wavelength of spectral band,
H_{pit}, V_{pit} = horizontal and vertical detector pitches in microns,
H_{det}, V_{det} = horizontal and vertical detector sizes in microns,
S_{scene} = electron flux per cm^2 due to scene,
$S_{enclose}$ = electron flux per cm^2 from enclosure,
S_{amp} = equivalent electron flux per cm^2 due to amplifier noise (calculated),
S_{drk} = electrons per cm^2 due to dark current (calculated),
A_{noi} = readout integrated circuit amplifier noise in electrons/pixel/frame (input),
D_{rk} = detector dark current in amperes per cm^2 (input),
σ_{vh} = fraction of flux equal to RMS fixed-pattern noise,
$F\#$ = f-number of objective lens,
F_{CS} = f-number of cold shield,
T_{CCD} = frame rate in Hertz (either 50 or 60 Hz),
E_{well} = maximum number of electrons in well,
$QE(\lambda)$ = quantum efficiency at wavelength λ,
λ_{pk} = λ with peak QE,
$D_{\lambda pk}$* = peak detectivity in Jones normalized per cm^2 and root-Hertz,
T_E = temperature of enclosure in Kelvin,
T_S = scene temperature in Kelvin,
τ = transmission of optics, and
β = absorption in optics.

The equivalent electron flux to generate amplifier noise in a square centimeter of detector area is given by Eq. (11.12):

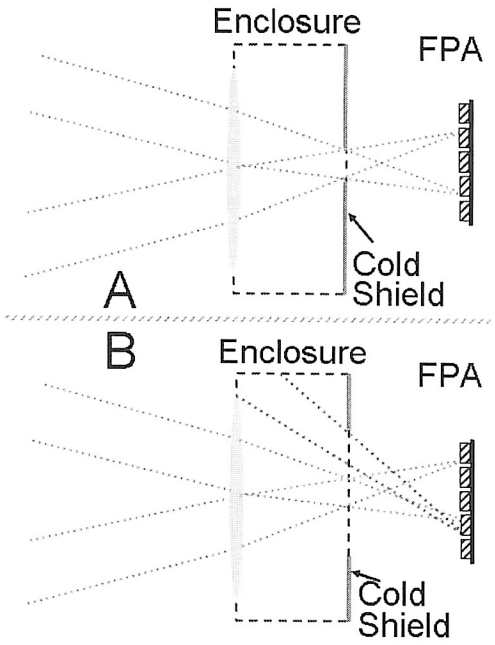

Figure 11.15 Illustration of detector cold shielding. The FPA is to the right of the figure. The cold shield is the barrier in the middle with a hole in it. The lens is to the left. In A (top), thermal flux from the enclosure is blocked by the cold shield. In B (bottom), the detector sees part of the enclosure, and flux from the enclosure increases detector noise.

$$S_{amp} = \frac{1\times10^{8}\, A_{noi}^{2}\, T_{CCD}}{H_{det}\, V_{det}}. \tag{11.12}$$

The equivalent electron flux for dark current is the dark current per cm^2 converted to electron flux by dividing by q_e:

$$S_{drk} = \frac{D_{rk}}{q_e}. \tag{11.13}$$

The electron flux due to the scene is

$$S_{scene} = \tau \int_{\lambda_1}^{\lambda_2} \frac{\mathrm{C1}\, QE(\lambda)\, d\lambda}{4\mathrm{C3}\lambda^{4}\left[\exp\left(\dfrac{C2}{\lambda T_S}\right)-1\right] F\#^{2}}. \tag{11.14}$$

The electron flux due to the enclosure is given by Eq. (11.15):[11]

The program is run by clicking on the *Run Program* button. Completion of program execution is indicated in two ways. First, the output file is opened automatically. This is shown in Fig. 11.17. Second, the *Graphs* button is enabled. Automatic opening of the output file is disabled by clicking on the *Output File Option* menu and selecting *Open file manually using* "*Open Output File*."

The program starts automatically running the *Thermal.txt* input file. Other input files are loaded or saved by clicking on the *File* menu. The *File* menu also has an exit selection, or the "X" at top right also exits the *Thermal* program.

The main purpose of the output file is to display the parameters calculated in the program. Parameters such as field of view (FOV), system magnification, sample spacing, and detector instantaneous FOV are listed. A short list of selected input parameters is also provided. In addition, the output file provides tables of MTF values.

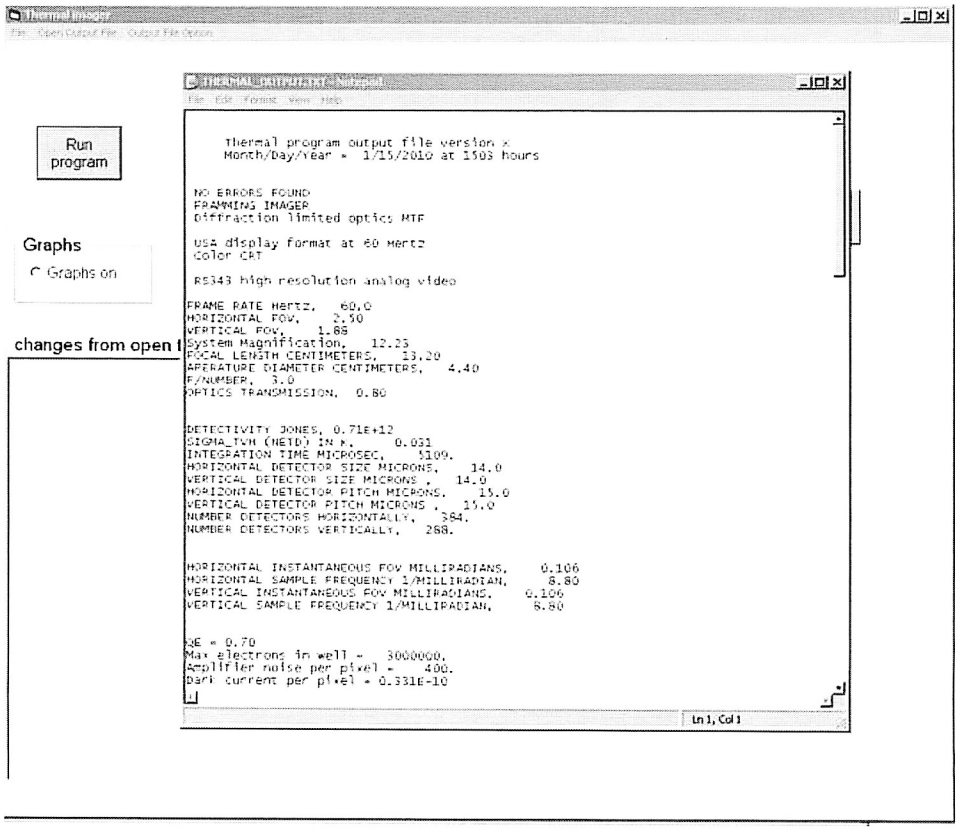

Figure 11.17 After the program executes, the output file is opened automatically and the *Graphs* option is enabled. Automatic opening of the output file is prevented by using the *Output File Option* menu.

Most program information is presented using the *Graphs* windows. Selecting *Graphs* after a run opens the window shown in Fig. 11.18. The pull-down box is used to select one of fourteen graph options:

1. Optics MTF,
2. Detector MTF,
3. Detector spectral response,
4. Digital & interpolate MTF,
5. Display MTF,
6. Horizontal pre, post, & system MTF,
7. Vertical pre-, post-, & system MTF,
8. System contrast threshold function,
9. Plot imager resolution,
10. Range plots,
11. Horizontal variable-gain MRT,
12. Vertical variable-gain MRT,
13. Horizontal aliasing, and
14. Vertical aliasing.

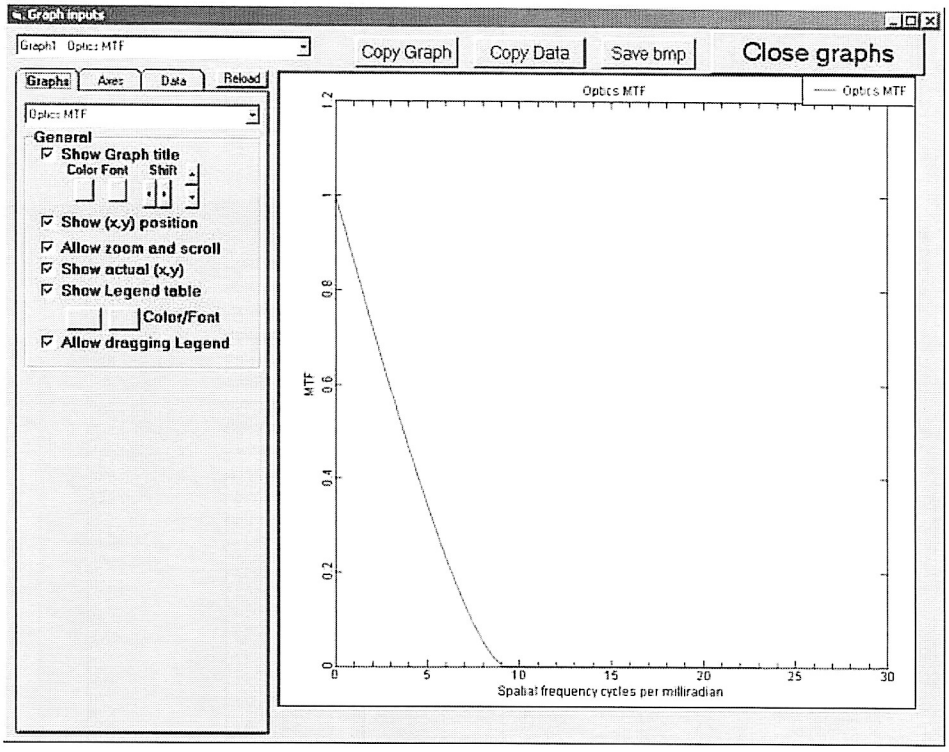

Figure 11.18 The *Graphs* window is the main source of information about the run. After selecting one of fourteen graphs, the user can copy both data and the graph using the Microsoft ClipBoard. The *Copy Graph* and *Copy Data* buttons are at the top of the window.

The model user creates output reports by selecting a graph and then clicking on *Copy Graph* or *Copy Data* and pasting the ClipBoard to Microsoft Excel or Word or another program that accepts the Microsoft ClipBoard.

Clicking on the *Lens* picture opens the input window shown at the left in Fig. 11.19. One of the options *ideal*, *good*, *typical*, or *input MTF array* is selected. The first three options enter MTF automatically. The input MTF array option makes the *Edit* button appear. Clicking on this button opens the window shown to the right in the figure. If an MTF array is entered, all frequencies must be monotonically increasing from top (1) to bottom. All MTFs must be between zero and one. The same MTF is applied horizontally and vertically.

The *OK* and *Cancel* buttons on the optics windows function the same as all other input windows. *OK* enters the data into the run file, and previous values are lost. *Cancel* returns all values to the state before the window was opened. The *Cancel* button on the main optics window (the window to the left in Fig. 11.19) also cancels new array inputs entered in the window at the right in Fig. 11.19.

Clicking on the *Focal Plane Array* picture opens the window shown in Fig. 11.20. Although this window looks complicated, the user can select an FPA from the drop-down lists. Selecting an FPA automatically enters all of the detector parameters. First an array type is selected from the following options:

InSb MWIR,
MCT MWIR,
MCT LWIR, and
QWIP
Uncooled.

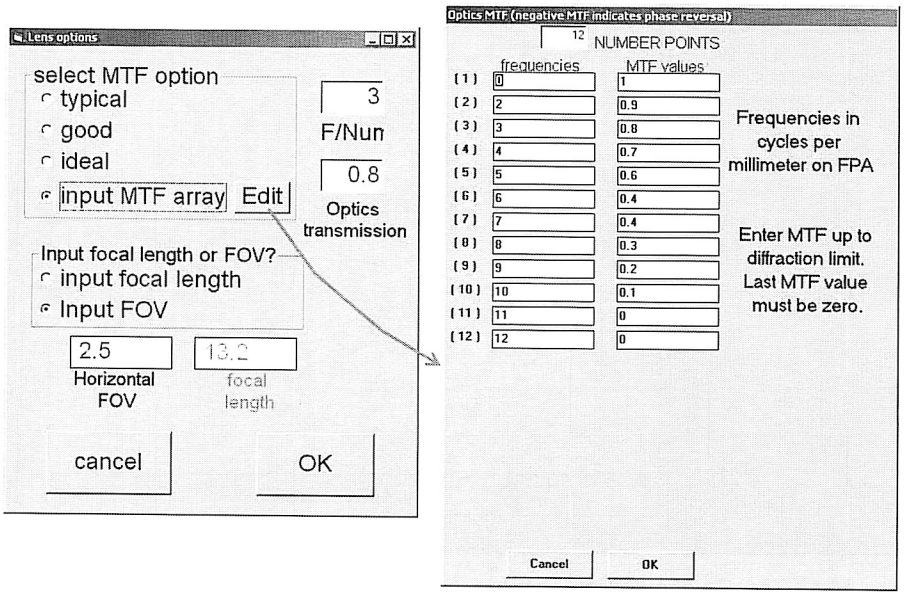

Figure 11.19 The main *Lens* window is on the left, and the array input window on the right. The user has an option of inputting either FOV or focal length (but not both). Whichever is input, the other is calculated by the program.

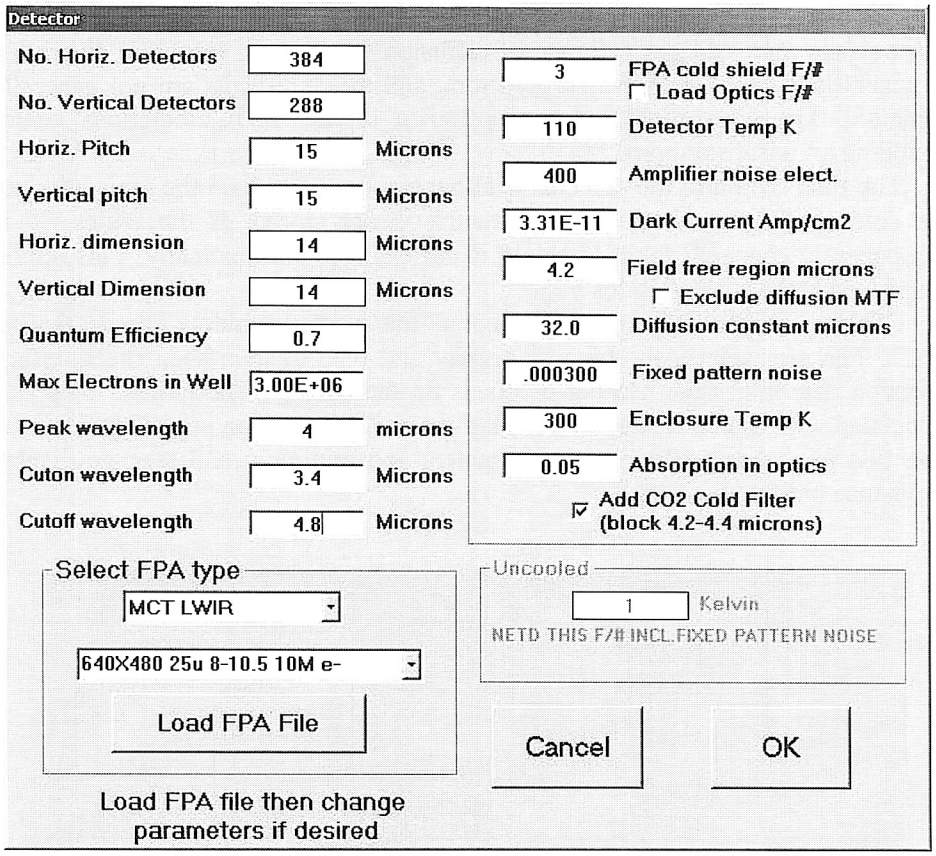

Figure 11.20 Screenshot of the *Detector* window. All input parameters can be input. Alternatively, the *Load FPA File* option is used. The user can also load the FPA file and then change any inputs before storing by clicking the *OK* button.

Then a specific array is selected from the second drop-down list. Clicking on the *Load FPA File* button loads the detector parameters. The user can accept all of the input detector parameters or change any or all of them. When the *OK* button is clicked, the program stores the values in these windows.

The *Uncooled* array type is different from the other detectors in that noise equivalent temperature difference (NETD) is entered. The measured NETD is for *f*/1 optics and optical transmission equal to one. In other words, NETD represents the array and not the current imager. Many of the input parameters disappear when *Uncooled* is selected. The *Thermal* program does not attempt to calculate the effect of environment on uncooled detectors.

The detector window also allows the user to select a carbon dioxide (CO_2) blocking filter. If selected, the program blocks 4.20- to 4.4-μm light from the detector. Since the atmosphere blocks light in this spectral band after only a few feet, allowing this flux on the detector increases noise without helping target signature. The blocking filter helps performance in the MWIR but does represent additional cost.

Another option in the detector window is to exclude diffusion MTF. The input arrays represent our estimate of diffusion parameters. However, this MTF is generally ignored for infrared detectors, and measurements are not generally available. The user might opt for optimism in the MTF predictions versus including an unsubstantiated MTF.

The final option in the detector window is a button to load the optics *f*/# into the cold shield *f*/#. Note that this switch is not stored. If the optics *f*/# is subsequently changed, the cold shield is not changed automatically. This option simply loads the current optics *f*/#.

Clicking on the *Display* picture opens the display window shown in Fig. 11.21. The user selects the type of display and type of interface. The interface selection determines the number of pixels on the display. The number of pixels associated with each interface format is given in Table 11.2 on page 218. The user also fills in viewing distance in centimeters and minimum and average display luminance in foot Lamberts.

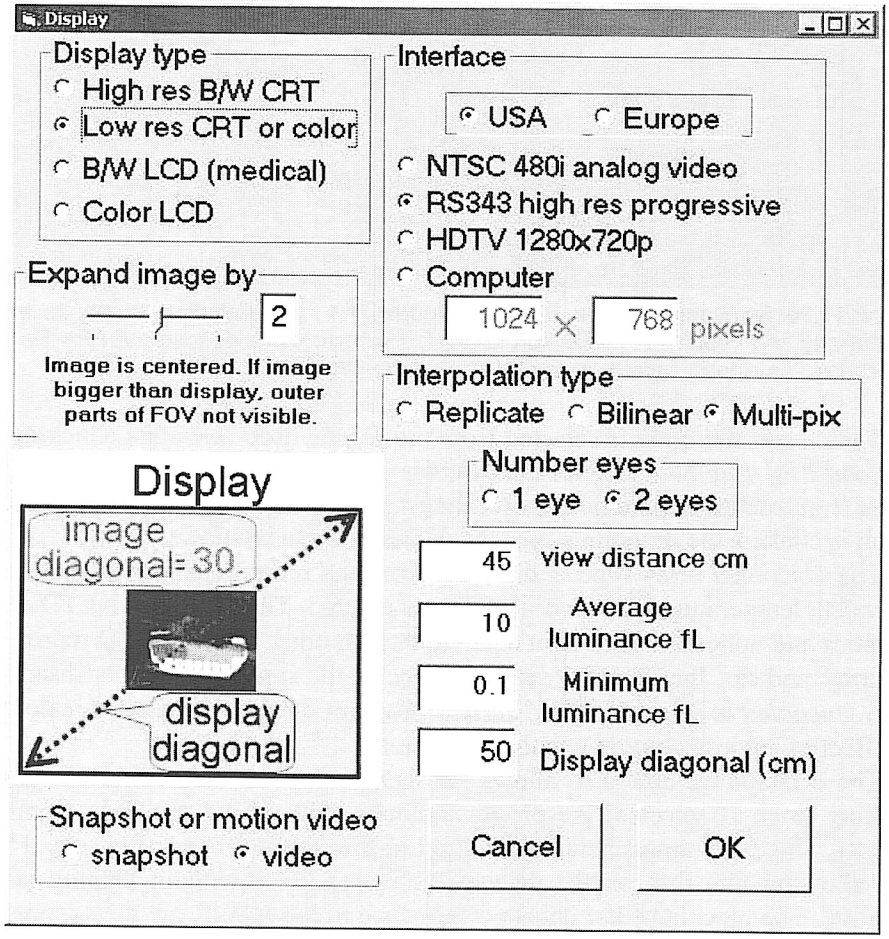

Figure 11.21 The *Display* window.

The display diagonal input is an important entry. This is the physical size of the display and not the sensor portion of the display area. The diagonal size is compared to the total pixels (determined by the interface format) to establish the size of the image. The following example illustrates how the various inputs interact.

In Fig. 11.21, a low-resolution display and RS343 analog video format are selected. Since display diagonal is 50 cm, the display height is 30 cm. A 3:4 aspect ratio is assumed if the display format is not HDTV. HDTV has a 9:16 aspect ratio. The CRT spot size is based on dividing 30 cm by 525 lines. Note that if a high-resolution CRT is selected, then the spot size would be based on 30 cm divided by 960 lines. Spot size is established by the display, not by the interface.

The FPA has 384 × 388 detectors. Since the display has 1280 × 960 pixels, the image diagonal without interpolation is 15 cm. However, as shown in the figure, the image is expanded by two. Therefore, the image diagonal is 30 cm. This value is shown superimposed on the display picture. Image diagonal is recalculated and updated each time the window input parameters are changed. If image size exceeds display size, then only the center portion of the image is displayed.

If the image is expanded by two or three, then the MTF associated with the selected interpolation technique is applied. Interpolation MTF is described in Chapter 4. *Multi-pix* interpolation uses the *6 samples* coefficients from Table 4.1 on page 91.

Clicking on the *Digital Filter* picture opens the window to the left in Fig. 11.22. If the answer to the question "Apply digital filter?" is "no," then no MTF is applied. If the answer is "yes," then the user indicates whether to apply the filter to FPA data or to interpolated data. If interpolation is not used (expand image by 1 in the display window), the FPA-versus-interpolate option makes no difference. To enter digital filter coefficients, the *Edit coefficients* button is clicked. This opens the window shown to the right in Fig. 11.22.

In the coefficient window, the user enters the number of coefficients for horizontal and vertical. Five coefficients are selected in the figure, but up to 20 can be entered. The user also selects whether the filters are *odd* or *even*. Figure 11.23 illustrates how the coefficients are applied for odd and even filters. Figure 11.22 shows *odd* selected for both filters. In Fig. 11.23, the horizontal filter is odd and the vertical filter is even.

Clicking on the *Extra Pre-and Post-MTF* button allows the user to input additional pre- and post-MTFs. Pre-MTFs are prenoise and presample blurs. Post-MTFs are postnoise and postsample blurs. The main window is shown to the left in Fig. 11.24. This window allows the user to independently select additional horizontal or vertical pre-MTFs or additional horizontal or vertical post-MTFs. The MTF is applied only if *Yes* is selected, regardless of the values in the associated array.

To input array values, click on *Edit*. This opens a window similar to the one at the right in Fig. 11.24. The figure shows twenty array inputs, but as few as two can be selected. All frequencies are in object space. The frequencies must be monotonically increasing from top (1) to bottom. Pre-MTFs must be between

zero and one ($0 \leq \text{MTF} \leq 1$). Pre-MTFs cannot apply gain. The array should span the frequency range to the diffraction limit. Regardless of the frequency span, however, the array must be extended such that the last MTF value is zero.

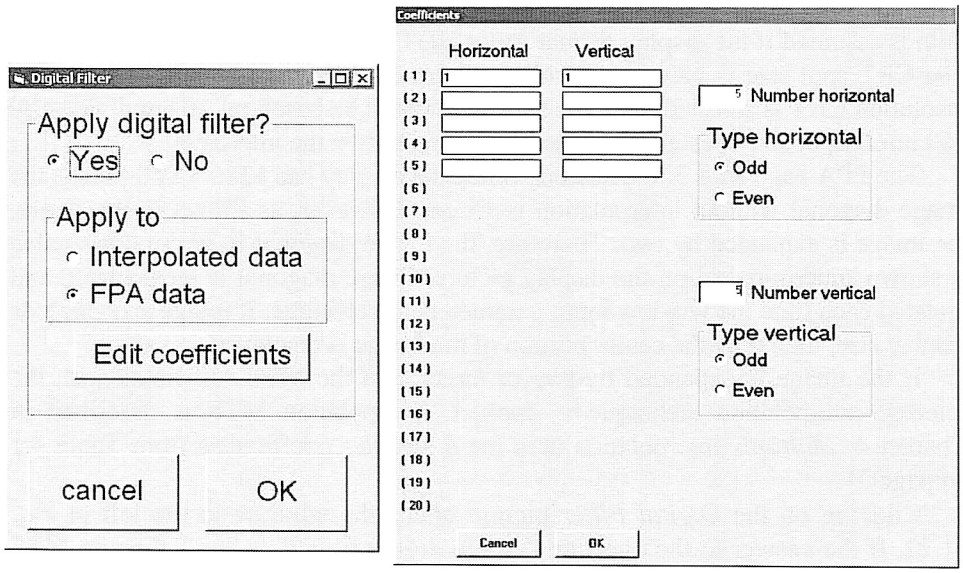

Figure 11.22 The main digital filter window is shown at the left. The window to enter digital coefficients is shown at the right. Up to 20 coefficients can be entered. Different coefficients can be applied horizontally and vertically.

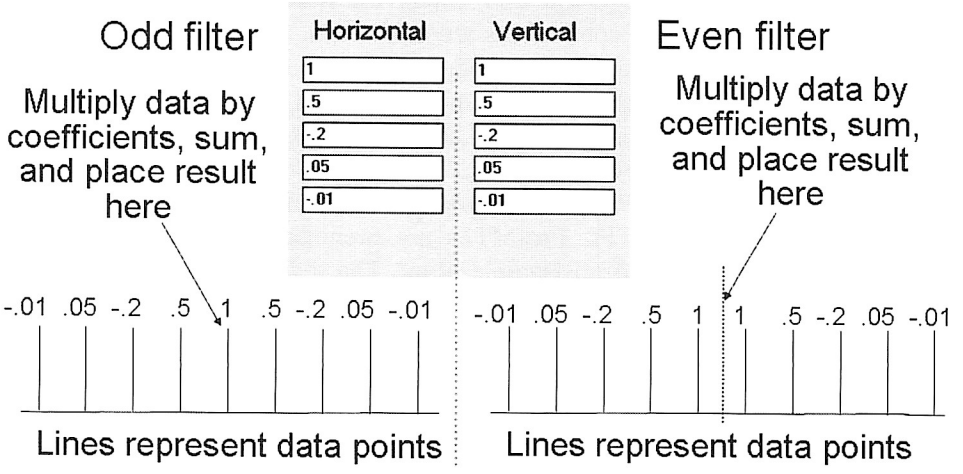

Figure 11.23 The meaning of *odd* and *even* filters is illustrated in this figure. For odd filters, the first coefficient is applied to the center data point. Other coefficients are applied symmetrically to either side. For even filters, a new data point is found by applying the coefficients symmetrically about a point between two original data points.

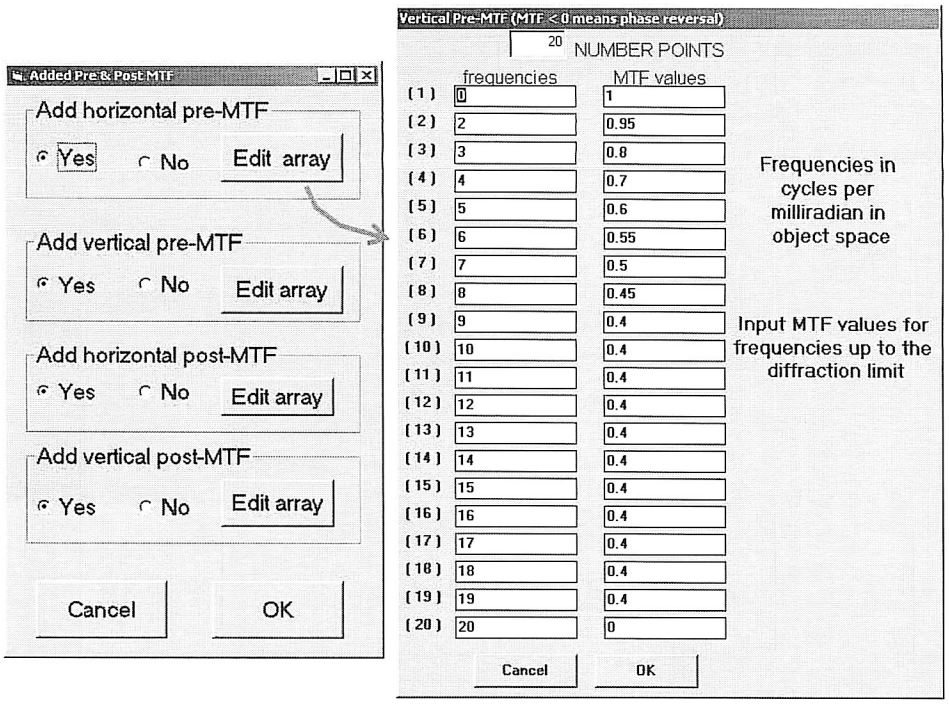

Figure 11.24 This window is used to insert additional MTFs. The MTFs are added only if *Yes* is clicked, regardless of the values in the associated array.

Post-MTF takes any value. Gain can be applied with post-MTF. Again, however, the last MTF value in the input array must be zero. This is because the program cannot extrapolate MTF; the frequency at which MTF goes to zero must be supplied.

11.6 Imager Analysis Using the Programs

Three of the *Graphs* windows are particularly useful for understanding imager behavior. The graphs are selected by clicking on *Graphs* in the main window and using the pull-down menu. The three windows are discussed in the following three sections.

11.6.1 Imager resolution

Figure 11.25 shows the *Plot imager resolution* window. The abscissa is target contrast T_{ebb} in effective blackbody Kelvin. The ordinate is cycles per milliradian resolution (the TTP metric). Imager gain is automatically adjusted as target contrast varies in order to maintain a 0.25 modulation contrast on the display. This contrast would result in saturating some pixels in a complex scene. This contrast setting is used in order to minimize the effect of the display.

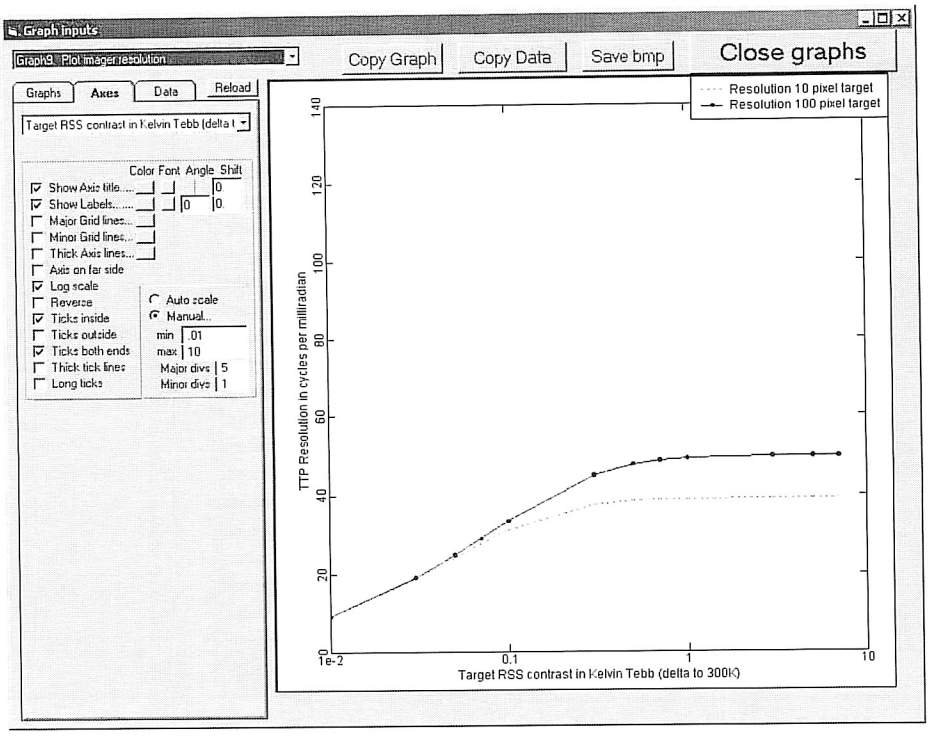

Figure 11.25 Screenshot of the *Plot imager resolution* window.

One curve plots the resolution of a 10-pixel target, and the second curve is for a 100-pixel target. Targets subtending many pixels are not affected by any aliasing in the imager. Targets that subtend only a few pixels are badly corrupted if aliasing is present. The separation between these curves indicates whether and how much aliasing is present.

Good resolution with high target contrast indicates good range performance against hot targets in good weather. The resolution at temperatures near 0.1 K indicates whether the imager performs in cold dreary weather.

11.6.2 System contrast threshold function

The window for *System Contrast Threshold Function* is shown in Fig. 11.26. The abscissa is spatial frequency in object space cycles per milliradian. The ordinate is contrast threshold. Horizontal and vertical are plotted separately. This plot is useful because it shows imager response versus spatial frequency.

The controls at the lower left allow the user to vary target size and contrast. As target contrast is varied, imager gain is adjusted to maintain 0.25 modulation contrast on the display. Decreasing target contrast increases noise because gain increases. Increased noise raises the entire threshold curve. Varying target size allows the user to see the effect of aliasing. When the target size is decreased, threshold increases at frequencies where aliased signal is present. Target contrast and size are noted on the graph and in the copy data.

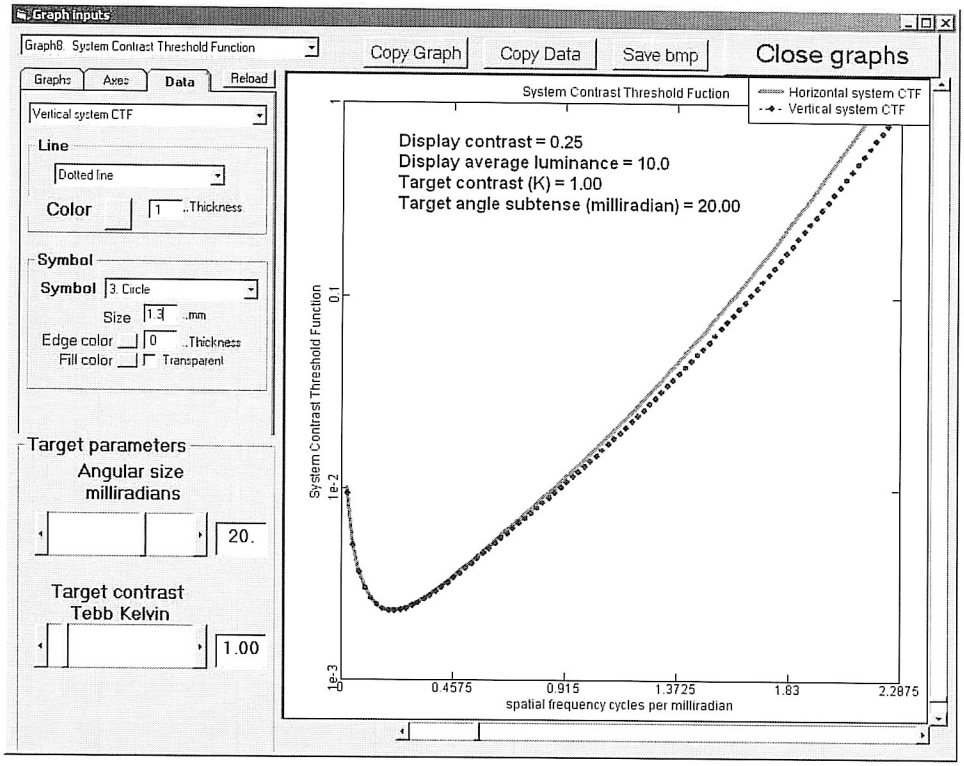

Figure 11.26 Screenshot of the *System Contrast Threshold Function* window.

11.6.3 Range plots

Figure 11.27 shows a PID-versus-range plot. The user adjusts target, background, and atmosphere input parameters using the controls at the lower left. Clicking on the *Calculate PID vs. range* button generates a range plot. An expanded view of the input controls is shown in Fig. 11.28. The notes in the figure explain the function of each control.

Target contrast can be in T_{ebb} or T_{pyro}. The delta temperature is centered at 300 K (T_{ebb}) or at the background temperature (T_{pyro}). These concepts are explained in Chapter 9. When the background is cold, the same value of T_{pyro}. has less energy than T_{ebb}. When the background is hotter than 300 K, T_{pyro} has more energy. Also, the spectral content of the two temperature types is different.

The ground temperature is automatically set when an atmosphere is selected. The ground temperature is set to the air temperature. The user can change the temperature to any value between 240 and 340 K.

Display contrast is given by Eq. (11.20). Imager gain is given by Eq. (11.21). S_{tmp} is scene contrast temperature in Kelvin. S_{tmp} is the scene temperature contrast that raises the display average luminance from black to average. S_{tmp} is not background temperature. The model assumes that the imager has sufficient gain to fill the display with detector noise.

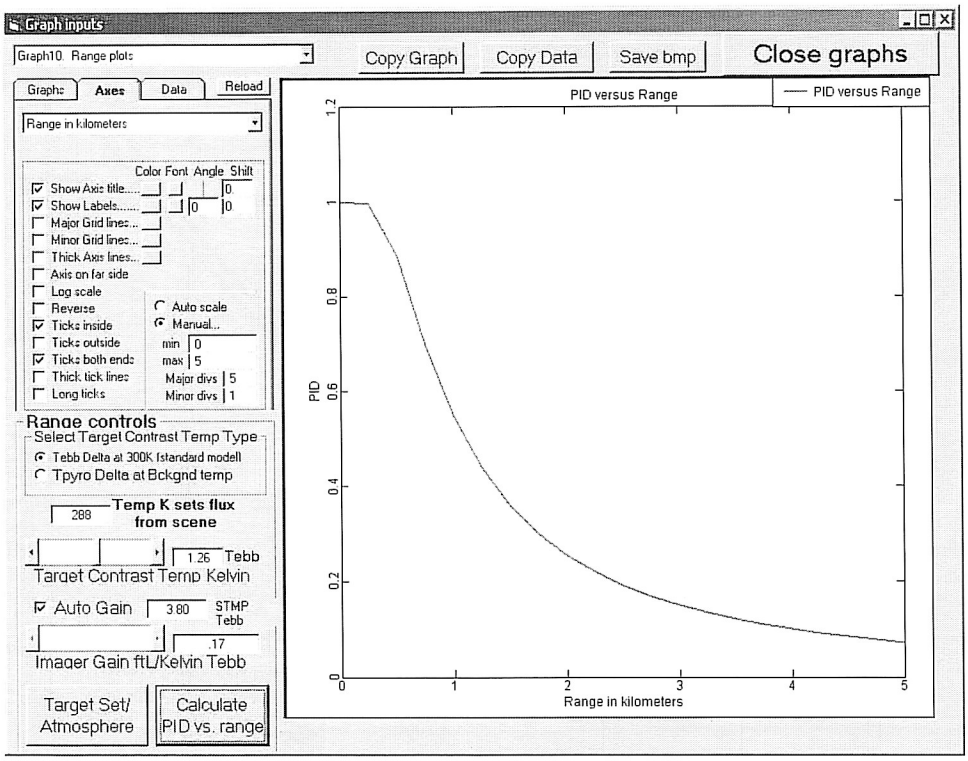

Figure 11.27 Input parameters are adjusted using the controls at the lower left. The range plot is generated by clicking on the *Calculate PID vs. range* button.

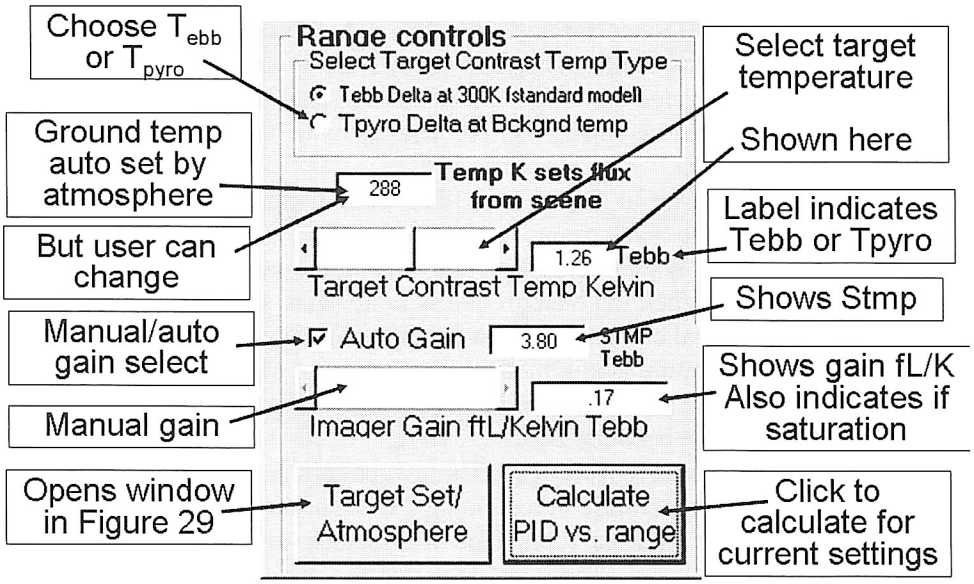

Figure 11.28 Screenshot showing the range controls that appear in the *Graph inputs* window when *Range plots* is selected. The added notes explain what each control does.

$$\text{display contrast} = \frac{\text{target contrast in Kelvin}}{2\ S_{tmp}\ \text{in Kelvin}}. \tag{11.20}$$

$$\text{imager gain} = \frac{\text{display average luminance in fL}}{S_{tmp}\ \text{in Kelvin}}. \tag{11.21}$$

Gain is automatically adjusted to keep S_{tmp} equal to a multiple of three of the target contrast. This maintains displays contrast at 0.17. If *Auto Gain* is turned off, gain is controlled manually by the horizontal slider. If gain is increased such that target contrast is greater than one-third S_{tmp}, the warning "clipping" is displayed in the gain window. If target contrast exceeds S_{tmp}, then the warning "saturation" is displayed. Note that range calculation proceeds, regardless of these warnings.

The 0.17 display contrast setting assumes a complex scene. This setting provides good contrast while avoiding saturation. For cold-soaked scenes, gain can be increased. However, a gain setting in which target contrast exceeds S_{tmp} is physically unrealistic.

When the button *Target Set/Atmosphere* is clicked, the window in Fig. 11.29 opens. This window is used to input target size and task difficulty. Atmosphere and turbulence are also selected using this window.

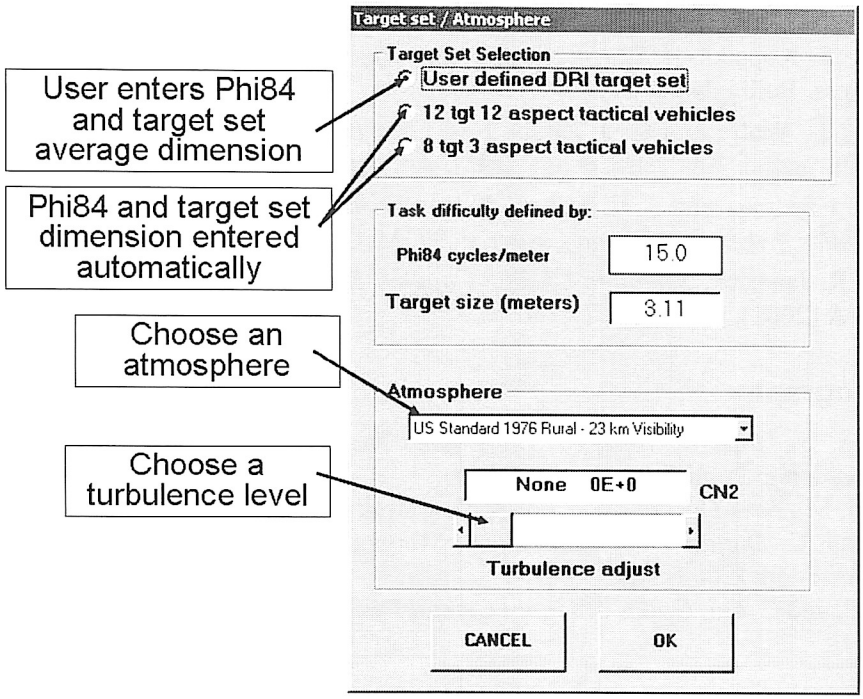

Figure 11.29 Target set size and task difficulty are input in the *Target set / Atmosphere* window. This window is also used to select atmospheres.

When all of the parameters are selected, click on the *Calculate PID vs. range* button located at the bottom left of the *Graphs* window. (See Fig. 11.27). The program calculates PID versus range and plots the results.

References

1. R. E. Fischer and B. Tadic-Galeb, *Optical System Design*, McGraw-Hill, New York (2000).
2. W. J. Smith, *Modern Lens Design*, McGraw-Hill, New York (2005).
3. L. E. Tannas, Jr., *Flat-Panel Displays and CRTs*, p. 175, Van Nostrand Reinhold Co., New York (1985).
4. R. G. Driggers, P. Cox, and T. Edwards, *Introduction to Infrared and Electro-Optical Systems*, p. 257, Artech House, Boston (1999).
5. R. L. Myers, *Display Interfaces*, *Wiley Series in Display Technology*, p. 132, John Wiley & Sons, Chichester, UK (2002).
6. W. den Boer, *Active Matrix Liquid Crystal Displays*, p. 143, Elsevier, Burlington, MA (2005).
7. G. Waldman and J. Wootten, *Electro-Optical Systems Performance Modeling*, p. 98, Artech House, Boston (1993).
8. K. Buskila, S. Towito, E. Shmuel, R. Levi, N. Kopeika, K. Krapels, R. G Driggers, R. H. Vollmerhausen, and C. E. Halford, "Atmospheric modulation transfer function in the infrared," *Appl. Opt.* **2**, 471–82, 14735966 (2004).
9. N. S. Kopeika, *A System Engineering Approach to Imaging*, p. 463, SPIE Press, Bellingham, WA (1998).
10. W. L. Wolfe and G. J. Zissis, Eds., *The Infrared Handbook*, The Infrared Information Analysis Center, ERIM, Ann Arbor, MI (1993).
11. E. Friedman and J. L. Miller, *Photonics Rules of Thumb: Optics, Electro-Optics, Fiber Optics, and Lasers*, p. 97, McGraw-Hill, New York (2004).
12. J. R. Janesick, *Scientific Charge-Coupled Devices*, SPIE Press, Bellingham, WA (2001).

Bibliography

Caniou. J., *Passive Infrared Detection: Theory and Applications*, Kluwer Academic Publishers, Boston (1999).

Laikin, M., *Lens Design*, CRC Press, New York (2007).

Poynton, C. *Digital Video and HDTV*, Morgan Kaufmann Publishers, Elsevier, New York (2003).

Yeh, P. and C. Gu, *Optics of Liquid Crystal Displays*, Wiley, New York (2010).